Volume 16, Number 2, 2023. pp. 181-194

Jordan Journal of Physics

ARTICLE

Green Synthesized TiO_2-SnO_2 Nanocomposite for the Photocatalytic Degradation of Methylene Blue Dye

Diptarka Roy[a], **AnilKumar Yadav**[a], **Kijay B. Singh**[b] and **Gajanan Pandey**[b]

[a] *Advanced Materials Research Laboratory, Department of Physics, Babasaheb Bhimrao Ambedkar University, Lucknow-226025, Uttar Pradesh, India.*
[b] *Department of Chemistry, Babasaheb Bhimrao Ambedkar University, Lucknow-226025, Uttar Pradesh, India.*

Doi: **https://doi.org/10.47011/16.2.6**

Received on: 15/08/2021; *Accepted on: 31/10/2021*

Abstract: TiO_2-SnO_2 nanocomposite was prepared by green synthesis method with the help of the *Allium sativum* extract obtained from garlic cloves. The green synthesized TiO_2-SnO_2 nanocomposite was characterized by XRD, SEM, EDS, Raman, ATR-FTIR, and UV-Visible spectroscopy. The XRD pattern reveals the polycrystalline nature of the synthesized nanocomposite and indicates the simultaneous presence of anatase and rutile phases of TiO_2, along with SnO_2. The calculated average crystallite size is 11.79 nm. The SEM images give the concept of surface morphologies of the synthesized nanocomposite. EDS spectrum detects the presence of Ti, Sn, and O in the synthesized nanocomposite material. The Raman spectrum confirms the chemical compositions. ATR-FTIR spectrum shows the presence of organic components of garlic as functional groups in the synthesized nanocomposite. The Tauc plot obtained from the UV-Visible spectral data displays the direct and indirect band gap values of 3.97 and 3.25 eV, respectively. Moreover, the present study investigates the effect of the synthesized nanocomposite's concentration on the photocatalytic degradation of methylene blue (MB) dye. The aqueous suspension of TiO_2-SnO_2 nanocomposite photocatalyst with a concentration of 1.5 mg/mL exhibits maximum photocatalytic activity.

Keywords: Green synthesis, TiO_2-SnO_2 nanocomposite, *Allium sativum* extract, Photocatalytic activity, Methylene blue.

1. Introduction

Photocatalytic activity is fundamentally the bandgap radiation, resulting from which electron-hole pairs are created [1-3]. Among the different photocatalysts, titanium dioxide (TiO_2) is one of the most efficient and prevalent materials with an extensive range of environmental applications, namely water and air purification, etc., due to its higher photosensitivity and photostability. Previous studies have shown that TiO_2 nanopowders have different crystal structures, surface areas, crystallite sizes, surface hydroxyl groups, etc., that depend on the synthesis routes [4-6]. The photocatalytic activities are deeply affected by those variations in their physical properties. Anatase crystallite shows comparatively higher photocatalytic activity [7]. As the adsorption capacity of anatase for organic pollutants is higher than the rutile, the anatase TiO_2 also displays significantly lower recombination rates than the rutile for its 10-fold more significant rate of hole trapping [8]. TiO_2 is an n-type semiconductor with good electrical conductivity, chemical stability, and unique optical

Corresponding Author: Anil Kumar Yadav **Email**: akyadavbbau@gmail.com

transparency [9]. TiO_2 heterostructure can enhance the electron-transfer process in photocatalysis. The mechanism of binary metal oxide photocatalyst, which has been described previously in many research articles, directs only a lower exciton recombination during the transfer of negatively charged carriers (electrons) from the conduction band to the valence band, thereby proving highly beneficial for the process of reducing organic pollutants. Several photocatalysts can obstruct the rapid recombination of exciton pairs through a range of diverse processes. The binary metal oxide semiconductor photocatalyst composed of tin oxide and titanium dioxide is very efficacious in reducing electron-hole recombination through Schottky barriers to the Fermi energy [10-13]. Tin oxide (SnO_2) is an n-type semiconductor with widespread applications in various capacities, for example, in sensors, energy storage, environmental remediation, etc. [14]. TiO_2-based nanocomposites are designed to enhance photocatalytic activity under the UV-visible region. The presence of SnO_2 in the nanocomposite contributes to the generation of more hydroxyl radicals compared to other materials. Considering the ionic radius and the structure (ionic radius 0.605Å for Ti^{4+} and 0.69Å for Sn^{4+} with tetragonal structure), TiO_2 and SnO_2 are almost analogous in nature. Titanium dioxide (TiO_2) has the energy bandgap value of 3.2 eV for the anatase phase, while for the rutile phase it is 3.0 eV. On the other hand, tin oxide (SnO_2) has an energy bandgap of 3.6 eV. The TiO_2-SnO_2 metal oxide composite photocatalyst can improve the charge carrier's lifespan by enhancing the charge difference within crystalline phases and reducing the charge recombination rate. In this composite system, electrons and holes occupy the conduction band of SnO_2 and the valence band of TiO_2, respectively. The photocatalytic activity of TiO_2-SnO_2 nanocomposite depends on the synthesis route and precursor's variety. Different synthesis routes can be followed to produce TiO_2-SnO_2 nanocomposites in the powder or film forms. These routes include sol-gel [15-16], co-precipitation [17], hydrothermal [18], chemical vapor deposition [19], spray pyrolysis [20], laser pyrolysis [21], and others. These conventional nanostructure synthesis techniques involve the use of complex and hazardous ingredients or chemicals. Additionally, these methods typically require enormous amounts of energy and costly instruments. Moreover, the byproducts generated during these processes are toxic and pose challenges to environmental sustainability. Green synthesis is a new alternative approach that links plants with nanoscience and nanotechnology and is a simple, environment-friendly technique to synthesize nanomaterials or nanocomposite using the extract of plant components as capping or reducing elements [22]. The photocatalytic activities of TiO_2-SnO_2 nanocomposite have been studied using several dyes, such as methylene blue, rhodamine B, and phenol [23]. Wastewater contains various organic pollutants, which have numerous negative environmental issues. Mostly, wastewater is generated by industrial processes that use organic dyes, such as textile manufacturing, food processing, furniture making, paint production, etc. Methylene blue is one of the commonly used dyes in these industries. Photocatalysis is a remarkable process of ecological cleanup and energy augmentation facilities, which can effectively degrade methylene blue [24].

The present study reveals the synthesis of TiO_2-SnO_2 nanocomposite using the *Allium sativum* (garlic) clove extract by following a self-designed green process. The synthesized nanocomposite was then evaluated for photocatalytic activity in degrading methylene blue (MB) dye.

2. Materials and Methods

2.1 Ingredients and Chemicals

Titanium (IV) chloride LR {$TiCl_4$, molecular weight (M.W.) 189.71 g/mol, purity 98%} from S D Fine Chem Limited, India and tin (II) chloride dihydrate {$SnCl_2$, $2H_2O$, M.W. 225.64g/mol, purity 97%} from Thermo Fisher Scientific India Pvt. Ltd. were used to synthesize TiO_2-SnO_2 nanocomposite. The *Allium sativum* bulbs (garlic) were purchased from the local market in the vicinity of the author's university. Ethyl alcohol (C_2H_6O, M.W. 46.069 g/mol, purity 99.9%) purchased from Chong Yu Hi-tech Chemicals, China) was used to prepare garlic extract as a precursor. Liquor ammonia (NH_3, 25%, M.W. 17.03 g/mol) from Thermo Fisher Scientific India Pvt. Ltd. was used during the nanocomposite synthesis process. Whatman filter paper (No.1, diameter 125 mm, Cat No. 1001125, GE Healthcare UK Limited) was used

for the filtration process during the garlic extract preparation and nanocomposite synthesis.

2.2 Green Synthesis of TiO_2-SnO_2 Nanocomposite

Firstly, the *Allium sativum* cloves (as shown in Fig. 1) were cleaned with double-distilled water and then dried at room temperature. Then, the garlic cloves were smashed with the help of mortar, and 10 grams of this smashed garlic was added to 20 mL of ethanol. Next, the mixture was heated at 60°C for 2 hours by using a hot plate. After that, the mixture was filtrated with Whatman filter paper to get the final extract solution. For synthesizing TiO_2-SnO_2 nanocomposite, 0.4 M titanium (IV) chloride and 0.02 M tin (II) chloride dihydrate solutions were prepared in ethanol separately. The magnetic stirring duration for the purpose was 6 hours for each case. After preparing precursor solutions separately, they were mixed up together and further stirred for another 6 hours with the help of the magnetic stirrer. Then 6.4 mL garlic extract was added to the final precursor solution (containing both the titanium and tin ions) by maintaining the weight-to-volume ratio (w/v) of the total precursor to the extract at approximately 1:1. The addition of garlic extract to the precursor solution resulted in the reduction of titanium and tin ions. This reduction was indicated by the color change of the precursor solution from transparent to yellowish-brown. During the reduction process, TiO_2-SnO_2 nanocomposite was produced. To get the nanocomposite as precipitate, 18 mL liquid ammonia (NH_3, 25%) was added to the final solution. The precipitate was collected by a filtration process using Whatman filter paper. The chloride ions present as an impurity were removed by washing the precipitate with double distilled water through filtration. After that, the precipitate was dried at room temperature and annealed at 550°C for 3 hours in a muffle furnace. To get TiO_2-SnO_2 nanocomposite powder, the annealed sample was gently rubbed with the help of an agate mortar pestle. The plausible reaction mechanisms related to the reduction of Ti^{4+} and Sn^{2+} ions by phytochemicals and the formation of TiO_2 and SnO_2 during the green synthesis of TiO_2-SnO_2 nanocomposite are represented in Fig. 2.

2.3 Characterization of Synthesized TiO_2-SnO_2 Nanocomposite

The crystalline nature of the synthesized TiO_2-SnO_2 nanocomposite was investigated by an X-ray diffractometer (BRUKER D8 Advance, Cu-Kα radiation wavelength λ = 0.154 nm) within the range2θ=10°-90°. The chemical assemblage and phase of the synthesized TiO_2-SnO_2 nanocomposite were predicted by a Micro Raman spectroscope (JobinYvonHoribra LABRAM-HR 800). The surface morphology of the synthesized nanocomposite material was studied by Scanning Electron Microscope (JEOL JSM-6490 LV), and the elemental analysis was performed by X-ray Energy-Dispersive Spectroscopy (EDS) (Oxford, INCAx-act). The functional groups present in the synthesized nanocomposite were detected by a Fourier Transform-Infrared spectrometer (FTIR) with an ATR spectrophotometer within the range between 4000-500 cm^{-1} (Brucker Alpha). The optical absorption and bandgap of the synthesized TiO_2-SnO_2 nanocomposite were studied with the help of a UV–Visible spectrophotometer (Evolution-201, Thermo Fisher Scientific). The photocatalytic activity was assessed by a UV-Visible spectrophotometer (CARRY-100).

FIG. 1. *Allium sativum* (garlic).

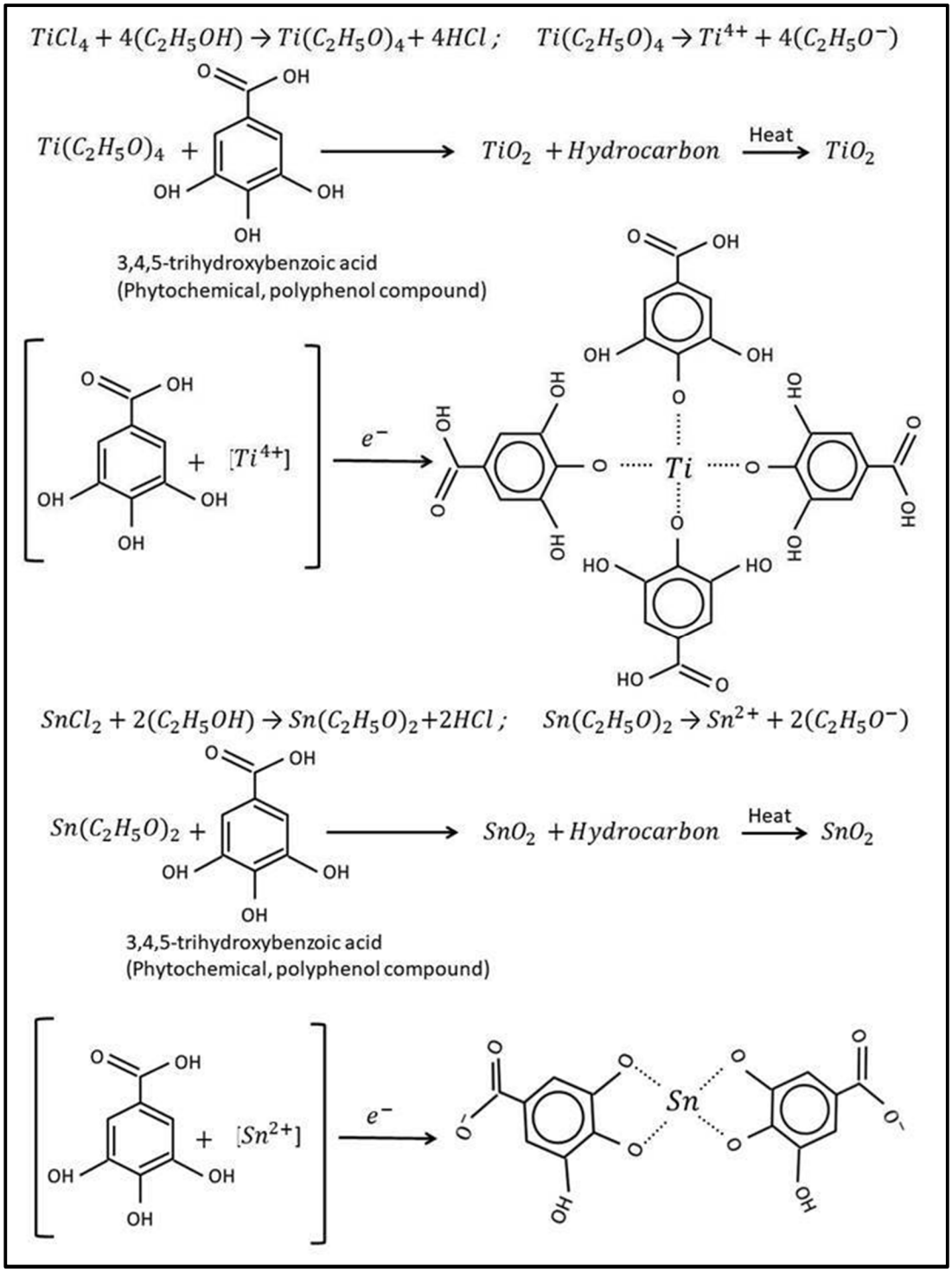

FIG. 2. The plausible reaction mechanism during the green synthesis of TiO_2-SnO_2 nanocomposite.

2.4 Photocatalytic Assessment of TiO_2-SnO_2 Nanocomposite for Methylene Blue Dye

The photocatalytic property of the prepared TiO_2-SnO_2 nanocomposite was examined through the degradation of methylene blue under direct sunlight. In this experiment, a freshly prepared methylene blue (MB) solution (20 ppm) was divided into five separate tubes, each containing 10 mL of the solution. A 3 mL aqueous suspension of catalyst at concentrations of 1.0, 1.5, 2.5, and 5.0 (in mg/mL) was added into 4 tubes, while one tube served as blank or control. All the reaction mixtures were sonicated at 30°C for being well mixed and to establish an equilibrium of the reaction mixture. After that, each suspension was put under direct sunlight

irradiation. The sunlight-driven degradation of MB in the presence of green synthesized TiO_2-SnO_2 nanocomposite catalyst was initially recognized by a steady decrease in the intensity of blue color. The progress of the degradation reaction of MB was also spectrophotometrically monitored between wavelength range 200-800 nm using supernatant part of filtered aliquots of reaction suspension at different time intervals. The degree of degradation or discoloration (%) of the MB solution was calculated by a relative alteration in the optical density of MB dye solution:

$$\% \text{ discoloration} = \frac{A_0 - A_1}{A_0} \times 100 \quad (1)$$

where A_0 represents the initial optical density of the MB solution at time t = 0, and A_1 is the final optical density at the end of the experiment, at time t [25].

3. Results and Discussion

3.1 XRD Spectroscopy

The XRD pattern of the synthesized TiO_2-SnO_2 nanocomposite is shown in Fig. 3. The peaks are situated at the 2θ positions 25.28°, 27.41°, 36.01°, 39.17°, 41.28°, 43.98°, 48.15°, 54.27°, 56.54°, 62.71°, 63.92°, and 68.99°. Those peaks are similar to the peaks reported in JCPDS card numbers 21-1276, 21-1272 for TiO_2 rutile and anatase phases, and 29-1484 for SnO_2. The resemblance of peak values with those JCPDS data indicates the polycrystalline nature of the synthesized titanium dioxide-tin oxide nanocomposite. The peak positions at 25.28° and 48.15° with the Miller indices (101) and (200), respectively, represent the anatase phase of TiO_2, indicating tetragonal crystal system with space group $I4_1/amd$ (141), and the lattice parameters such that $a = b = 3.7852\ Å,\ c = 9.5139\ Å$. The peak positions at 27.41°, 36.01°, 39.17°, 41.28°, 43.98°, 54.27°, 56.54°, 62.71°, and 68.99° have the Miller indices (110), (101), (200), (111), (210), (211), (220), (002) and (301), respectively indicate the rutile phase of TiO_2, which are related to the tetragonal crystal system with space group $P4_2/mnm$ (136), and the lattice parameters such that $a = b = 4.5933\ Å, c = 2.9592\ Å$ [JCPDS card: 21-1276, 21-1272, 29-1484]. The peak at 63.92° with Miller indices (311) indicates the SnO_2, which relates to the orthorhombic crystal system with lattice parameters $a = 4.714\ Å,\ b = 5.727\ Å,\ c = 5.214\ Å$. The average crystallite size of the synthesized nanocomposite can be determined using the Debye-Scherrer equation. The equation is given below:

$$D = \frac{0.89\lambda}{\beta \cos\theta} \quad (2)$$

where λ is the wavelength of X-ray, β is the full width at half the maximum of the X-ray diffraction line, θ is the Bragg diffraction angle, and the numerical value 0.90 is a factor that relates to the crystallite shape of the synthesized material [26]. As per the equation mentioned above, the calculated average crystallite size of the synthesized nanocomposite is 11.79 nm.

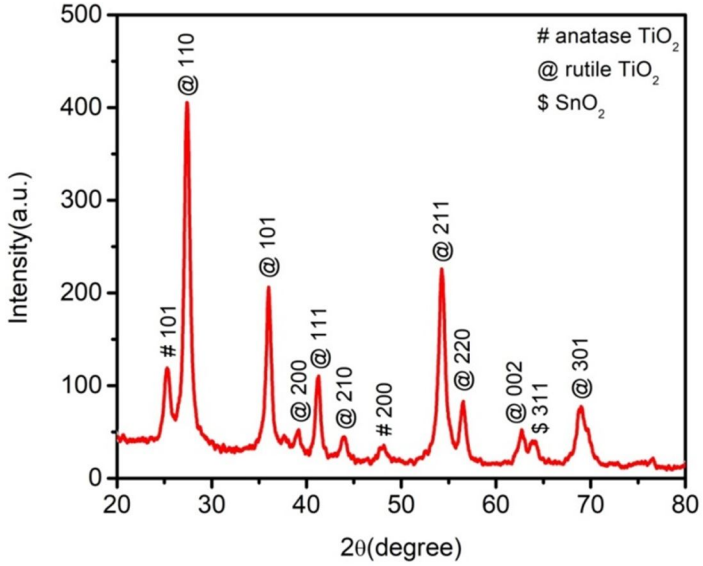

FIG.3. X-ray diffraction pattern of the synthesized TiO_2-SnO_2 nanocomposite.

3.2 Scanning Electron Microscopy (SEM)

The SEM images of the synthesized TiO_2-SnO_2 nanocomposite are represented in Fig. 4. These images help to explore the morphological characteristics of the synthesized material. The SEM images show the multi-grain agglomeration with unequal shapes and sizes, where large particles can be seen consisting of small grains [27]. However, the smaller grains apparently seem like semi-spherical shapes. The larger grains with different shapes and sizes indicate the simultaneous existence of anatase and rutile structures [28].

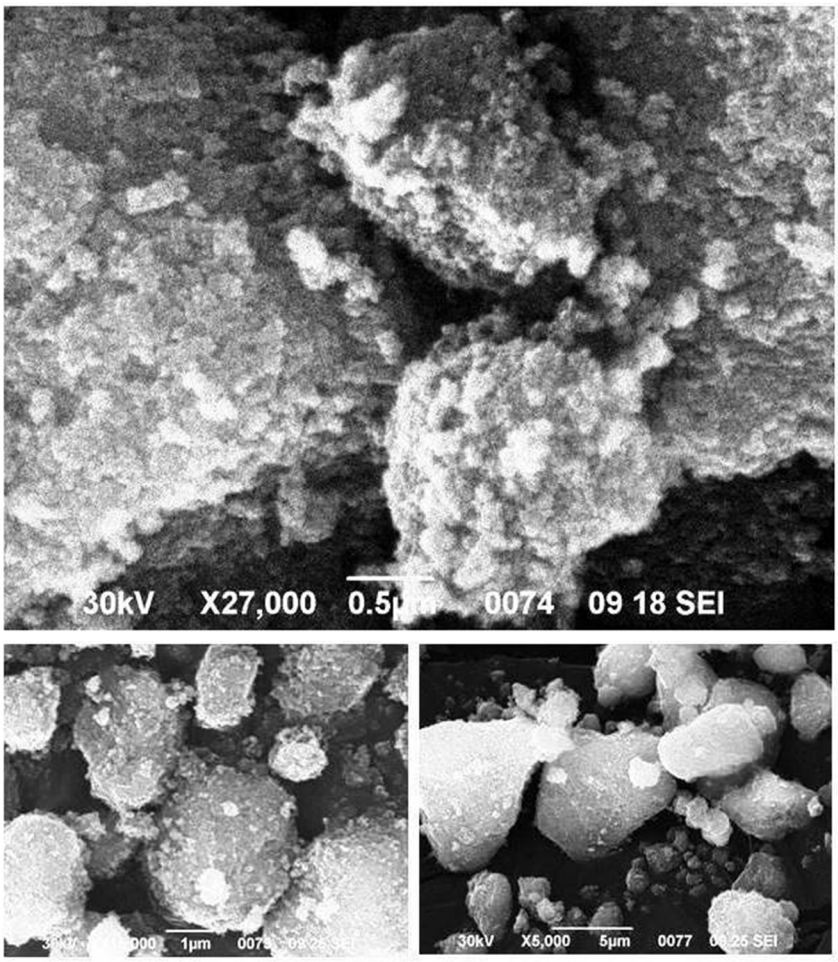

FIG. 4. The SEM images of the synthesized TiO_2-SnO_2 nanocomposite.

3.3 X-ray Energy Dispersive Spectroscopy (EDS)

The EDS spectrum of the synthesized TiO_2-SnO_2 nanocomposite is shown in Fig. 5. The EDS spectrum confirms the presence of metallic Ti and Sn, along with the O that indicates the formation of TiO_2-SnO_2 composite material. The presence of carbon in the synthesized TiO_2-SnO_2 composite signifies the contribution of organic compounds that belong to the phytochemical components of *Allium sativum*, used during the synthesis process [29]. As the X-ray energy dispersive spectroscope is attached to the Scanning electron microscope. Platinum (Pt) coating is used to create a conducting layer on the sample during the SEM imaging process to improve image quality. That is why Pt is present in the TiO_2-SnO_2 nanocomposite sample that is detected by the EDS spectrum.

3.4 Raman Spectroscopy

The Raman spectrum of the prepared TiO_2-SnO_2 nanocomposite is shown in Fig. 6. The bands in the Raman spectrum at 146, 400, 520, and 642 cm^{-1} represent the Raman active modes E_g, B_{1g}, A_{1g}, and E_g, respectively, for anatase TiO_2 [30]. The band at 146 cm^{-1} indicates O-Ti-O symmetric stretching vibration. Also, the bands at 400, 520, and 642 cm^{-1} correspond to the O-Ti-O symmetric bending, O-Ti-O asymmetric bending, and O-Ti-O symmetric stretching vibrations, respectively. Assimilation of SnO_2

and TiO_2 lattice forms the bonds such as Sn-O-Ti and Sn-O-Sn, which causes a reduction in the crystallite size, eventually lowering the peak intensities [31]. The band at 240 cm^{-1} detects the optical phonon mode (E_u) of SnO_2. Also, the band at 610 cm^{-1} represents the Raman active mode A_{1g} for the TiO_2 rutile phase. SnO_2 influences the growth of TiO_2 as a rutile phase than the anatase due to the structural resemblance between them in the nanocomposite [32-33]. Furthermore, the band at 446 cm^{-1} defines the E_g mode for the rutile phase of TiO_2 [34]. Thus, the characteristic Raman bands in the spectrum indicate the coexistence of anatase TiO_2, rutile TiO_2, and SnO_2 in the synthesizedTiO_2-SnO_2 nanocomposite.

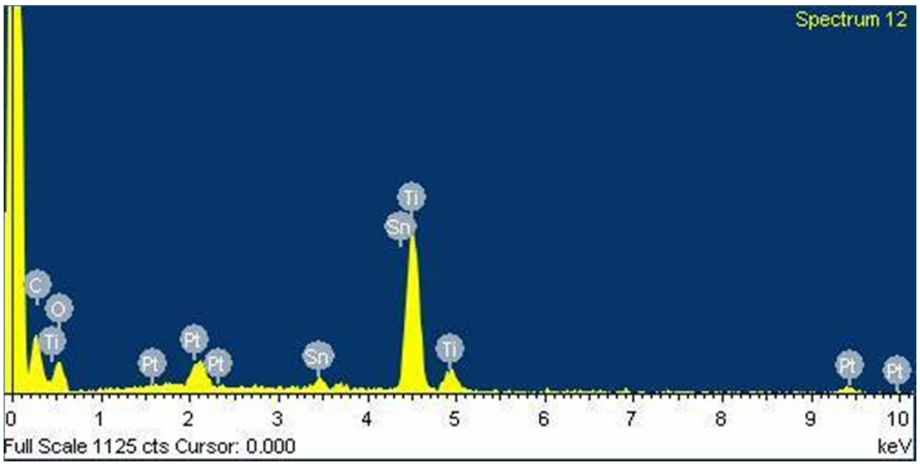

FIG. 5. EDS spectrum of the synthesized TiO_2-SnO_2 nanocomposite.

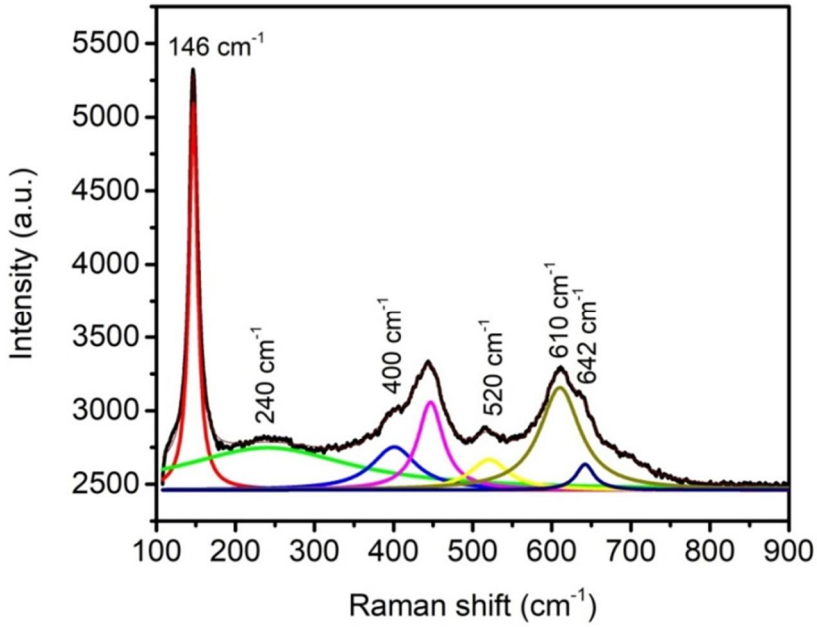

FIG. 6. Raman spectrum of synthesized TiO_2-SnO_2 nanocomposite.

3.5 FTIR Spectroscopy

The FTIR spectrum of the synthesized TiO_2-SnO_2 nanocomposite is shown in Fig. 7. The infrared absorption bands for SnO_2 and TiO_2 are generally detected at a position near about or below 600 cm^{-1} [35], which are not detectable in the FTIR spectrum recorded by the FTIR spectrometer attached with an ATR spectrophotometer. Furthermore, ligands are attached to the metal atoms by constructing a coordination complex that can be detectable by FTIR spectrum for a particular synthesized material. The phytochemicals from the garlic extract act as capping and reducing agents that is attached to metal atoms after reducing metal ions during TiO_2-SnO_2 nanocomposite formation. Some of those phytochemicals remain as functional groups with the synthesized TiO_2-SnO_2 nanocomposite even after the annealing process. Garlic extract contains proteins, carbohydrates, polyphenols, free amino acids,

polysaccharides, lignin, etc. The peak at 1515 cm^{-1} is associated with the symmetric stretch of the aromatic groups for lignin. The peak position at 1642 cm^{-1} relates to the stretching vibrations of aliphatic and aromatic double bonds. The peak at 1264 cm^{-1} may be ascribed by amide -III bands relates to the combination of C-N stretch and N-H bend for the peptide groups. The peak position at 1056 cm^{-1}, which lies in between the spectral range from 900 to 1200 cm^{-1}, originates from the coupling of C-C, C-O stretch and C-O-H, C-O-C deformation of oligo and polysaccharides. The peak at 2889 cm^{-1} is related to the asymmetric C-H stretch [36-37]. The peak at 3740 and 2332cm^{-1} may have arisen due to OH stretching and NH stretching vibrations [38].

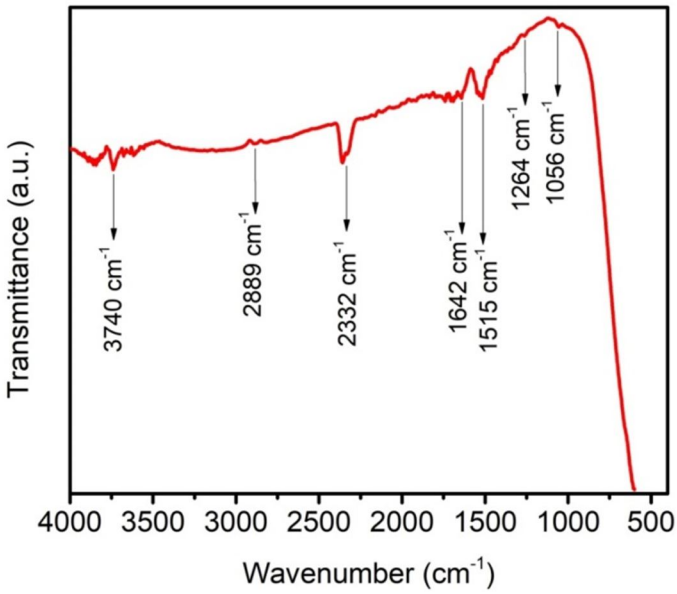

FIG. 7. FTIR spectrum of the synthesized TiO_2-SnO_2 nanocomposite using garlic extract.

3.6 UV-Visible spectroscopy

The optical absorption spectrum of the synthesized TiO_2-SnO_2 nanocomposite in the UV-Visible and the corresponding Tauc plots are depicted in Fig. 8. The bandgap of the sample was calculated using the equation given below, which is the combination of the Kubelka–Munk and Tauc relations:

$$\alpha h\nu = A(h\nu - E_g)^n \quad (3)$$

where, $\alpha = \frac{(1-R)^2}{2R}$ (4)

where h is the Planck's constant, $h\nu$ is the photon's energy, A is a constant which is independent of photon's energy, E_g is the optical bandgap, α is the Kubelka–Munk function, which is also called the coefficient of absorbance, R is the reflectance, and the values of n differ such that $n=2$ and $n = \frac{1}{2}$ indicate the indirect and direct transitions, respectively. The plot $h\nu$ versus $(\alpha h\nu)^m$, where $m = \frac{1}{n}$, helps to estimate the optical bandgap of the synthesized nanocomposite material [39-40]. From the UV-Visible absorption spectra [Fig. 8(a)], a strong absorption peak and a minor peak are identified at 234 and 270 nm, which belong to the UV-C region (200-280 nm) [41]. The calculated direct and indirect bandgap values from the Tauc plots [Figs. 8(b) and 8(c)] are 3.97 and 3.25 eV, respectively. However, the indirect transition provides a more accurate estimation of the bandgap energy (E_g) than the direct transition for any synthesized semiconductor material. Thus, indirect bandgap is recommended as the actual bandgap of the synthesized TiO_2-SnO_2 nanocomposite [42]. The bandgap value obtained from the Tauc plot depends on the crystallite size of the synthesized material. Smaller crystallite size exhibits higher bandgap energy, which a comparative study indicates in Table 1. The direct bandgap energy obtained from the Tauc plot is slightly higher than the previously reported value, indicating the smaller crystallite size of the synthesized TiO_2-SnO_2 nanocomposite material [43].

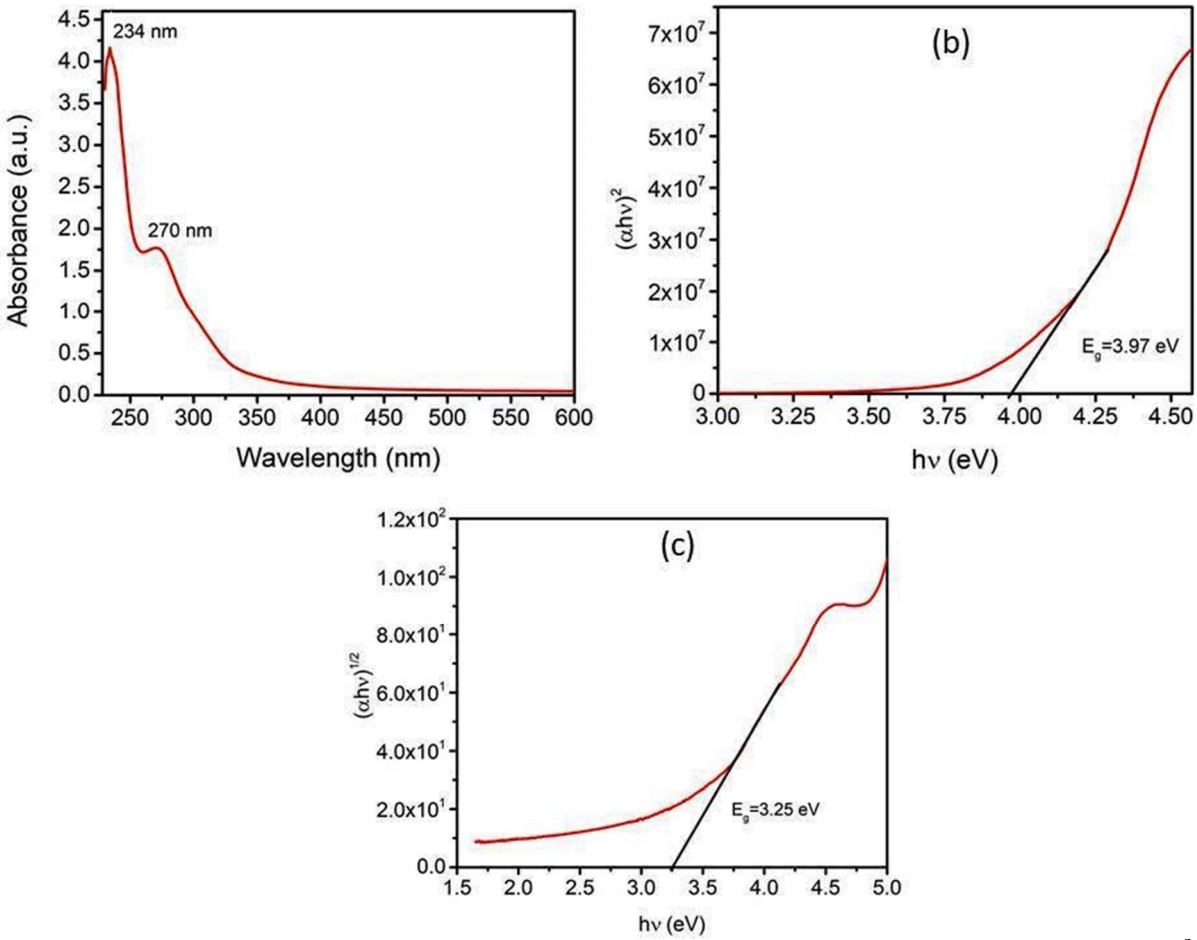

FIG. 8. (a) UV–Vis absorption spectrum of the synthesized TiO_2-SnO_2 nanocomposite; (b) plot of $h\nu$ Vs. $(\alpha h\nu)^2$ for the direct transition; (c) plot of $h\nu$ Vs.$(\alpha h\nu)^{\frac{1}{2}}$ for the indirect transition.

TABLE 1. Variation of band gap with crystallinity for green synthesized, and others previously reported TiO_2-SnO_2 nanocomposite material.

Synthesis method	Band gap (eV)	Crystallite size (nm)	References
Solid phase extraction (SPE)	3.4	60.5	[43]
Sol-gel	3.3 3.0 2.7	55.8 59.2 66.8	[44]
Pulsed laser deposition	2.9-4.1	65-35	[45]
Spray pyrolysis deposition	3.8	36	[46]
Sol-gel (co-precipitation) Mechanical mixing	3.0-4.0	23-4 23-12	[47]
Sol-gel	3.2-3.8	20-5	[48]
Green synthesis	3.9	11.7	Present work

3.7 Photocatalytic Activity

The catalytic efficacy of synthesized TiO_2-SnO_2 nanocomposite was analyzed by the photodegradation of dye (MB) under direct sunlight. The degradation was examined by recording the absorption spectrum of the reaction mixture at different time intervals in the wavelength range of 200-800 nm (Fig. 9).

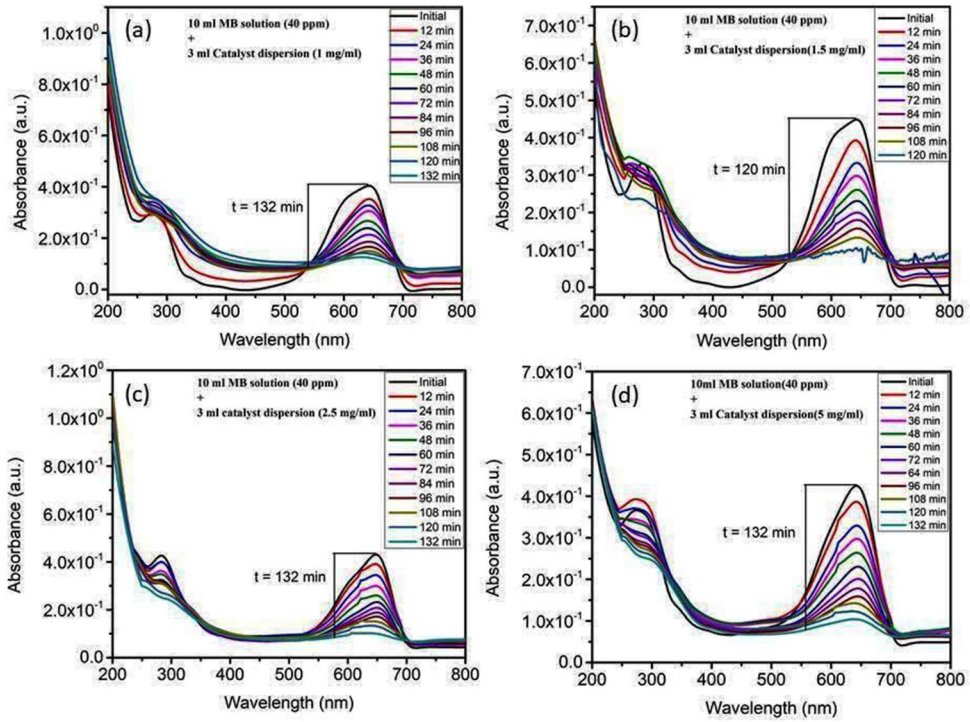

FIG. 9. Photodegradation of MB dye under solar light irradiation using 3 mL of aqueous suspensions of synthesized TiO_2-SnO_2 nanocomposite photocatalyst with concentrations (a) 1 mg/mL, (b) 1.5 mg/mL, (c) 2.5 mg/mL,(d) 5.0 mg/ml in the 10 mL of MB solution (20 ppm) for each case.

The absorption spectra of MB consists of maximum absorbance at 645 nm, characteristic of the MB dye. About 3 mL of aqueous suspensions of TiO_2-SnO_2 nanocomposite photocatalyst (1, 1.5, 2.5, 5.0 mg/mL) were mixed with 10 mL of MB solution (20 ppm) separately and placed in direct sunlight. The degradation of MB in an aqueous solution using TiO_2-SnO_2 nanocomposite photocatalyst was analyzed through UV-visible spectra between the wavelength range 200-800 nm. The UV-visible spectrum indicates a decrease in dye concentration with time during the photocatalytic process. The surface plasmon resonance (SPR) completely disappeared within 132, 120, 132, and 132 minutes when catalyst concentrations were 1.0, 1.5, 2.5, and 5.0 mg/mL with degradation values of 70.7%, 80.0%, 79.0%, and 76.7%, respectively. The obtained data were best fitted in pseudo-first-order kinetics; the rate constant was found to be 0.009, 0.01173, 0.1034, and 0.01064 min^{-1} for 1, 1.5, 2.5, and 5.0 mg/mL, catalyst loading. The pseudo-first-order kinetic plots are shown in Fig. 10.

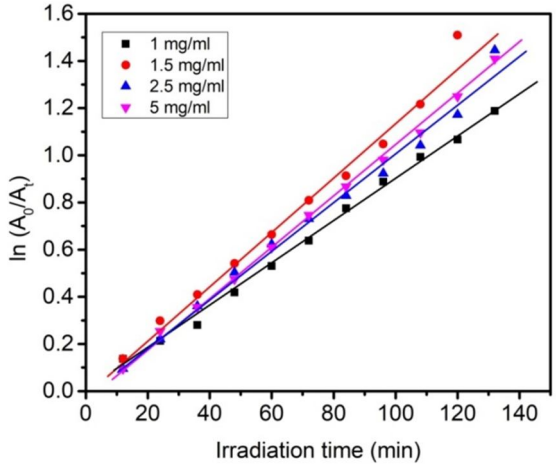

FIG. 10. First-order kinetic plots for the photodegradation of MB for 3 mL of aqueous suspensions of synthesized TiO_2-SnO_2 nanocomposite photocatalyst with concentrations 1 mg/mL, 1.5 mg/mL, 2.5 mg/mL, and 5.0 mg/mL in the 10 mL of MB solution (20 ppm) for each case.

The result of photocatalytic activity indicates the rapid degradation of MB in the existence of a TiO_2-SnO_2 nanocomposite catalyst. However, a significant impact on the catalyst concentration was observed, and the highest degradation rate was at 1.5 mg/mL. These data prove that TiO_2-SnO_2 photocatalyst enhances photocatalytic performance. The photocatalyzed degradation of MB dye for different concentrations of TiO_2-SnO_2 nanocomposite photocatalyst is schematically represented in Fig. 11.

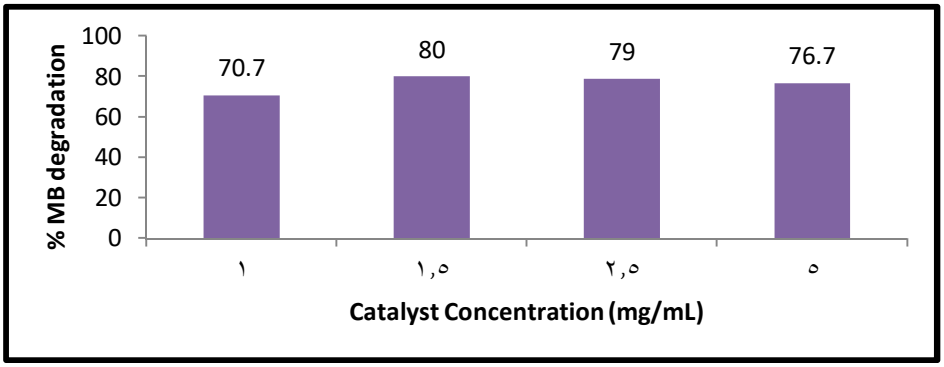

FIG. 11. Photodegradation percentage of MB dye for different concentrations of synthesized TiO_2-SnO_2 nanocomposite photocatalyst.

The plausible pathway for photocatalytic degradation of methylene blue in aqueous solution has been reported by Kavitha et al.:

$SnO_2 + h\nu \rightarrow h^+ (VB) + e^- (CB)$ (5)

$TiO_2 + h\nu \rightarrow h^+ (VB) + e^- (CB)$ (6)

$H_2O + h^+ \rightarrow H^+ + OH^\bullet$ (7)

$O_2 + e^- (CB) \rightarrow O_2^{-\bullet}$ (8)

$O_2^{-\bullet} + 2H_2O + 2e^- (CB) \rightarrow 3OH^- + OH^\bullet$ (9)

$OH^- + h^+ (VB) \rightarrow OH^\bullet$ (10)

$MB + OH^\bullet \rightarrow$ Degradation product (11)

$MB + h^+ \rightarrow$ Degradation product (12)

A comparison between green synthesized TiO_2-SnO_2 nanocomposite material and all other previously reported composite materials for the photocatalytic degradation of MB dye is represented in Table 2.

TABLE 2. A comparison between green synthesized TiO_2-SnO_2 nanocomposite material and other previously reported composite materials for the photocatalytic degradation of MB dye.

S. No.	Photocatalyst	Concentration of MB dye (mg/L)	Irradiation source	% degradation	Degradation time	Refs.
1	$Cu_2O/BiVO_4$	25	Visible light	72.9	160 min	[49]
2	CeO_2/V_2O_5	10	Visible light	76.9	300 min	[50]
3	aα-$Fe_2O_3/SiO_2/SnO_2/TiO_2$	25	UV light	-	120 min	[51]
4	Ni-Cu-Zn ferrite@SiO_2@TiO_2	20	35 W-Xe arc lamp	69	360 min	[52]
5	Fe_3O_4@MIL-100 (Fe)	40	500 W-Xe lamp	99	200 min	[53]
6	SnO_2@TiO_2 nanopillars	3.2	UV light	~90	480 min	[54]
7	Green TiO_2-SnO_2 nanocomposite	20	Direct sunlight	80	120 min	Present work

4. Conclusions

A green synthesis approach was used to prepare TiO_2-SnO_2 nanocomposite using the *Allium sativum* extract prepared from garlic cloves. The phytochemicals in that extract solution are beneficial for the metal ion reduction process and are also used as capping agents during nanocomposite synthesis. In the present work, the degradation of MB has been carried out in direct sunlight irradiation without using UV lamps, electrical equipment, and any oxidizing or reducing agent. The green synthesized TiO_2-SnO_2 photocatalyst has shown brilliant activity in degrading MB in the aqueous solution. In the photocatalysis process, the valence band electrons could be promoted to the conduction band of oxides of Sn and Ti due to solar light irradiation. This resulted in the simultaneous and equal creation of holes in the valence band. The SnO_2 of the photocatalyst accumulates the liberated electrons in the conduction band while the TiO_2 accumulates the holes, achieving a stable electronic state. Moreover, the electrons accumulated by SnO_2 could be captured by adsorbed O_2 molecules to generate reactive $O_2^{-\bullet}$ radicals mainly responsible for the degradation of MB in the aqueous solution. As far as we know, the present study is probably the first reported work associated with the photocatalytic degradation of MB dye by the green synthesized TiO_2-SnO_2 nanocomposite using the *Allium sativum* extract.

Funding

This research received no external funding.

Acknowledgments

Author Mr. Diptarka Roy is very thankful to the University Grant Commission (UGC), Government of India (GOI), New Delhi, India, for the financial support to accomplish doctoral research work. We are thankful to UGC-DAE Consortium for Scientific Research, Indore, M.P.-452017, India, for providing XRD and Laser Raman characterization facilities. Thanks to Prof. B. C. Yadav, Head, Department of Physics and Director, USIC, Babasaheb Bhimrao Ambedkar University, Lucknow, U.P.-226025, for providing UV-Visible spectroscopy and SEM facility. Thanks to Dr. Kamlesh Pandey, NCEMP, University of Allahabad, Prayagraj, U.P- 211002, India for providing the ATR FTIR spectroscopy facility.

Conflicts of Interest

The authors declare no conflict of interest.

References

[1] Kim, S.P., Choi, M.Y. and Choi, H.C., Mater. Res. Bullet., 74 (2016) 85.

[2] Shi, L., Zhang, Z., Wang, R., Zhou, C. and Sun, C., Ceram. Inter., 46 (2020) 19460.

[3] Oliveira, M.C., Fonseca, V.S., Andrade Netoa, N.F., Ribeiro, R.A.P., Longo, E., de Lazaro, S.R., Motta, F.V. and Bomio, M.R.D., Ceram. Inter., 46 (2020) 9446.

[4] Lettieri, S., Pavone, M., Fioravanti, A., Amato, L.S. and Maddalena, P., Materials, 14 (7) (2021) 1645.

[5] Crişan, M., Ianculescu, A.C., Crişan, D., Drăgan, N., Todan, L., Niţoi, I. And Oancea, P., Nanotechnology in the Beverage Industry, 2020 (2010) 265.

[6] Reghunath, S., Pinheiro, D. and Devi KR, S., Appl. Surf. Sci., 3 (2021) 100063.

[7] Inagaki, M., Nonaka, R., Tryba, B. and Morawski, A.W., Chemosphere, 64 (2006) 437.

[8] Sakthivel, S., Hidalgo, M.C., Bahnemann, D.W., Geissen, S.U., Murugesan, V. and Vogelpohl, A., Appl. Catal. B: Environment, 63 (2006) 31.

[9] Dobrzański, L.A., Szindler, M.M., Szindler, M., Lukaszkowicz, K., Drygała, A. and Prokopiuk vel Prokopowicz, M., Arch. Metall. Mater., 61 (2016) 833.

[10] Kaviyarasu, K., Magdalane, M., Jayakumar, D., Samson, Y., Bashir, A.K.H., Maaza, M., Letsholathebe, D., Mahmoud, A.H. and Kennedy, J., J. King Saud Univ. Sci., 32 (2020) 1516.

[11] Chaudhary, K., Shaheen, N., Zulfiqar, S., Sarwar, M.I., Suleman, M., Agboola, P.O., Shakir, I. and Warsi, M.F., Synthetic Met., 269 (2020) 116526.

[12] Aadil, M., Rahman, A., Zulfiqar, S., Alsafari, I.A., Shahid, M., Shakir, I., Agboola, P.O., Haider, S. and Warsi, M.F., Adv. Powder Technol., 32 (2021) 940.

[13] Magdalane, C.M., Kanimozhi, K., Arularasu, M.V., Ramalingam, G. and Kaviyarasu, K., Surface. Interfac., 17 (2019) 100346.

[14] Yuliarto, B., Gumilar, G. and Septiani, N.L.W., Adv. in Mater. Sci. Eng., 2015 (2015) 694823.

[15] Wang, Q., Wei, X., Dai, J., Jiang, J. and Huo, X., Mater. Sci. Semiconduct. Proces., 21 (2014) 111.

[16] Kutuzova, A.S. and Dontsova, T.A., Appl. Nanosci., 9 (2019) 873.

[17] Anandan, S., Pugazhenthiran, N., Lana-Villarreal, T., Lee, G.-J. and Wu, J.J., Chem. Eng. J., 231 (2013) 182.

[18] Liu, N., Chen, X., Zhang, J. and Schwank, J.W., Catalysis Today, 225 (2014) 34.

[19] Rasoulnezhad, H., Kavei, G., Ahmadi, K. and Rahimipour, M.R., Appl. Surface Sci., 408 (2017) 1.

[20] Wittawat, R., Rittipun, R., Jarasfah, M. and Nattaporn, B., Mater. Today Communicat, 24 (2020) 101126.

[21] Scarisoreanu, M., Fleaca, C., Morjan, I., Niculescu, A.M., Luculescu, C., Dutu, E., Ilie, A., Morjan, I., Florescu, L.G., Vasile, E. and Fort, C.I., Appl. Surf. Sci., 418 (2017) 491.

[22] Gebreslassie, Y.T. and Gebretnsae, H.G., Nanoscale Res. Lett., 16 (2021) 1.

[23] Hassan, S.M., Ahmed, A.I. and Manna, M.A., J. Sci.: Adv. Mater. Device, 4 (2019) 400.

[24] Kavitha, S., Jayamani, N. and Barathi, D., Bullet. Mater. Sci., 44 (2021) 26.

[25] Bharati, B., Sonkar, A.K., Singh, N., Dash, D. and Rath, C., Mater. Res. Exp., 4 (2017) 085503.

[26] Goutam, S.P., Saxena, G., Singh, V., Yadav, A.K., Bharagava, R.N. and Thapa, K.B., Chem. Eng. J., 336 (2018) 386.

[27] Messaadi, C., Ghrib, M., Chenaina, H., Manso-Silvan, M. and Ezzaouia, H., J Mater. Sci.: Mater. Electron., 29 (2018) 3095.

[28] Medjaldi, F., Bouabellou, A., Bouachiba, Y., Taabouche, A., Bouatia, K. and Serrar, H., Mater. Res. Express, 7 (2020) 016439.

[29] Santhoshkumar, J., Venkat Kumar, S. and Rajeshkumar, S., Resourc. Efficient Technol., 3 (2017) 459.

[30] Zhu, X., Jan, S.S., Zan, F., Wang, Y. and Xia, H., Mater. Res. Bullet., 96 (2017) 405.

[31] Prabakaran, S., Nisha, K.D., Harish, S., Archana, J., Navaneethan, M., Ponnusamy, S., Muthamizhchelvan, C., Ikeda, H. and Hayakawa, Y., Appl. Surfac. Sci., 498 (2019) 143702.

[32] Hirata, T., Ishioka, K., Kitajima, M. and Doi, H., Physic. Rev. B., 53 (1996) 8442.

[33] Medjaldi, F., Bouabellou, A., Bouachiba, Y., Taabouche, A., Bouatia, K. and Serrar, H., Mater. Res. Express, 7 (2020) 016439.

[34] Huang, M., Yu, J., Li, B., Deng, C., Wang, L., Wu, W., Dong, L., Zhang, F. and Fan, M., J. Alloy. Comp., 629 (2015) 55.

[35] Sasikala, R., Shirole, A., Sudarsan, V., Sakuntala, T., Sudakar, C., Naik, R. and Bharadwaj, S.R., Int. J. Hydro. Energ., 34 (2009) 3621.

[36] Biancolillo, A., Marini, F. and D'Archivioc, A.A., J. Food Composit. Analys., 86 (2020) 103351.

[37] Lu, X., Ross, C.F., Powers, J.R., Aston, D.E. and Rasco, B.A., J. Agric. Food Chem., 59 (2011) 5215.

[38] Amatya, S.P. and Pradhan Joshi, L., BIBECHANA, 17 (2020) 13.

[39] Bitaraf, M., Ghazi, M.E. and Izadifard, M., Cryst. Res. Technol., 55 (3) (2020) 1900145.

[40] Chetri, P., Basyach, P. and Choudhury, A., Chem. Phys., 434 (2014) 1.

[41] Dadvar, S., Tavanai, H. and Morshed, M., J. Nanopart. Res., 13 (2011) 5163.

[42] Lo´pez, R. and Go´mez, R., J. Sol-Gel Sci., Technol., 61 (2012) 1.

[43] Rahman, M.M., Khan, S.B.,Marwani, H.M. and Asiri, A.M., J. Taiwan Instit. Chem. Eng., 45 (2014) 1964.

[44] Sönmezoğlu, S., Arslan, A., Serin, T. And Serin, Necmi, Phys. Scr., 84 (2011) 065602.

[45] Rashed, S.H., Haider, A.J. and Younis, S., Eng. &Tech. J., 32 (B) (2014) 658.

[46] Mohammad, J.F. and Mohammed, R.I., Conf. Ser.: Mater. Sci. Eng., 928 (2020) 072073.

[47] Kusior, A., Zych, L., Zakrzewska, K. and Radecka, M., Appl. Surface Sci., 471 (2019) 973.

[48] Talinungsang, Paul, N., Purkayasthaa, D.D. and Krishna, M.G., Superlat. Microstruc., 129 (2019) 105.

[49] Min, S., Wang, F., Jin, Z. And Xu, J., Superlatt. Microstruc., 74 (2014) 294.

[50] Saravanan, R., Joicy, S., Gupta,V.K., Narayanan,V. and Stephen, A.J.M.S., Mater. Sci. Eng. C., 33 (2013) 4725.

[51] Chen, J.S, Chen, C., Liu, J., Xu, R., Qiao, S.Z. and Lou, X.W., Chem. Communic., 47 (2011) 2631.

[52] Chen, C.C., Jaihindh, D., Hu, S.H. and Fu, Y.P., J. Photochem. Photobiol. A: Chem., 334 (2017) 74.

[53] Zhang, C.F., Qiu, L.G., Ke, F., Zhu, Y.J., Yuan, Y.P., Xu, G. S. and Jiang, X., J. Mater. Chem. A., 1 (2013) 14329.

[54] Cheng, H.E., Lin, C.Y. and Hsu, C.M., Appl. Surf. Sci., 396 (2017) 393.